Electronic Supplementary Material (ESI) for Energy Advances.

Supporting Information
Facile Surface Engineering of Bio-Waste Derived Amorphous Carbon with SnO_2 Nanowires to Enhance the Efficacy of Li/Na Storage

S. Praveen Kumar, Balla Rekha Madhuri, Katchala Nanaji, Srinivasan Anandan, Tata Narasinga Rao and Ramkrishna Sahoo*

Centre for Nanomaterials, International Advanced Research Centre for Powder Metallurgy and New Materials (ARCI), Hyderabad-500005, Telangana, India.
Corresponding Author: ramkrishna.s@project.arci.res.in (Dr. Ramkrishna Sahoo)

Physical Characterization:

X-ray diffraction (XRD) data for all the synthesized samples were performed using Bruker AX D8 with Cu K_α radiation ($\lambda = 1.5405$ Å). Field-emission scanning electron microscope (FESEM) was carried out using Zeiss, Gemini-SEM 500 equipped with energy dispersive spectroscopy (EDS) detector (Octane elite plus, EDAX). X-ray photoelectron spectroscopy was performed by ESCA-Omicron XPS system with Mg Kα as the excitation source. BET surface area and BJH adsorption-desorption study of the samples were carried out by Micromeritics ASAP 2020 analyzer where degassing performed at 250 °C for 6 h before the measurements.

Physicochemical characterization:

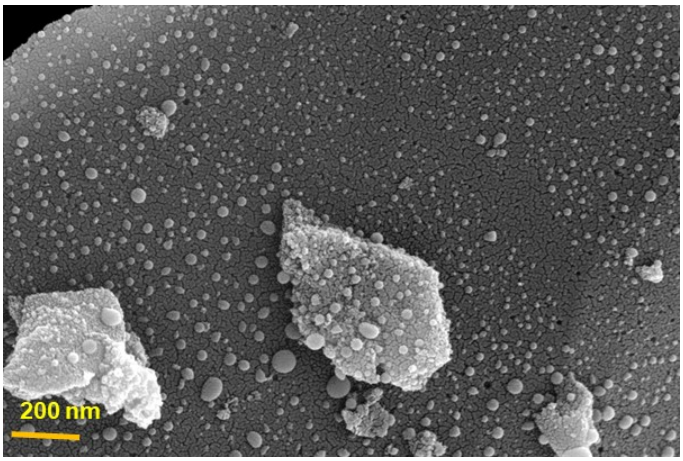

Fig. S1: FESEM image of the Carbon-SnO_2 physical mixture (P-C/SnO_2)

In Figure S2B, it can be seen that the NAC exhibits two distinct peaks, at 1335 cm^{-1} and 1588 cm^{-1} which defines the D band (attributes to the state of disorder in the carbon structure) and G band (signifies the in-plane vibration of the carbon atoms). Here it can be seen that the I_D/I_G ratio for NAC is 1.02 that signifies the disordered type of the as-prepared carbon. The I_D/I_G ratio increases to 1.1 in case of the C/SnO_2 composite representing the enhancement in the state of disorder in the carbon of the C/SnO_2 composite. Figure S2C and D depict the nitrogen adsorption-desorption isotherm curves for NAC and C/SnO_2 composite, respectively. The pattern of the isotherms for both samples follow mixed nature of type I (acute raise in nitrogen adsorption at <0.3 P/P_0) signifying the microporous character and type IV (hysteresis above 0.3 P/P_0) which stands for the presence of mesoporous character of the composite (Figure 2C and D). The calculated BET surface area of NAC is 434.19 m^2 g^{-1} (with microspore surface area of 341.12 m^2 g^{-1}) and that of C/SnO_2 is 402.19 m^2 g^{-1} (having microspore surface area 298.53 m^2 g^{-1}). The pore size distribution curve features that both NAC and C/SnO_2 are having pore diameters in the range ~1.8-1.9 nm and ~3.8-3.84 nm respectively suggesting the micro and mesoporous nature of the as-prepared samples (Figure S2E and F). The total pore volume of NAC and C/SnO_2 are 0.206 cm^3 g^{-1} and 0.217 cm^3 g^{-1}, respectively. The above results convey that C/SnO_2 exhibits almost similar adsorption-desorption behavior like NAC registering that the decoration of SnO_2 on the carbon surface does not contribute towards the porosity generation on the surface of the composite. The

mesoporous nature of the C/SnO_2 surface may play a pivotal role during the electrochemical reactions by providing facile pathway for metal ions.

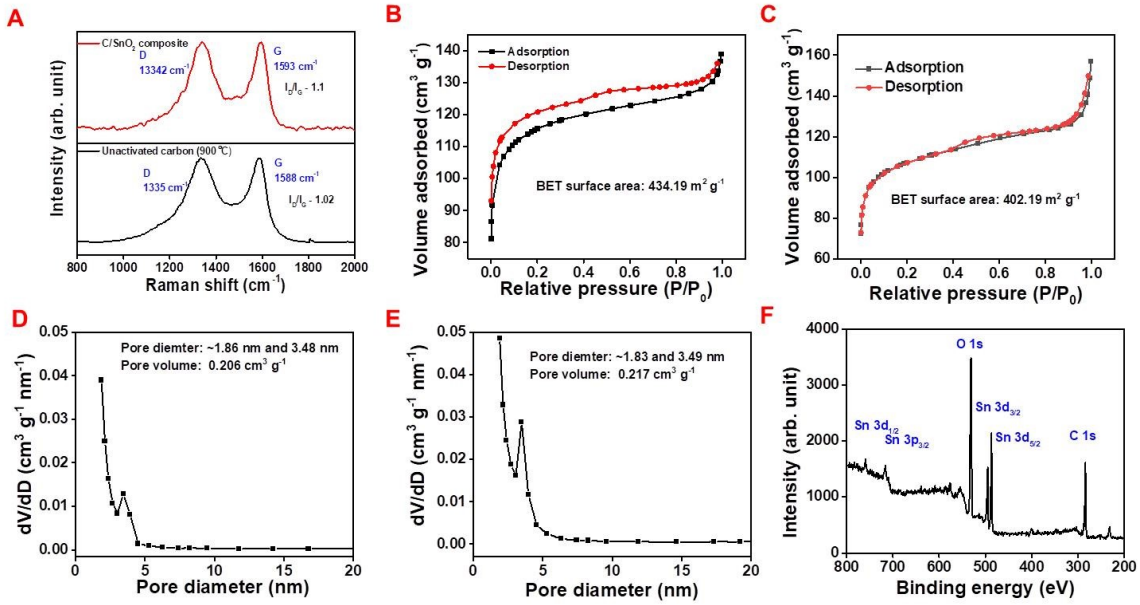

Figure S2: (A) Comparative Raman spectra of NAC (black line) and C/SnO_2 composite, N_2 adsorption-desorption isotherm (B) non-activated carbon (NAC) and (C) C/SnO_2 composite. Pore-size distribution curve of (D) non-activated carbon (NAC) and (E) C/SnO_2 composite. (F) Wide-range X-ray photo electron spectroscopy of C/SnO_2 composite,

Electrochemical analysis:

The P-C/SnO_2 composite delivers specific discharge and charge capacity of 1666 and 647 mA h g^{-1} having ICE of 39% at the specific current of 25 mA g^{-1} (Figure S3A). However, the capacity decreases abruptly in the 2nd and 3rd cycles where the calculated discharge/charge capacity values are 690/484 and 505/392 mA h g^{-1} having CE of 69% and 78%, respectively (Figure S3A). Cyclic stability of this as-prepared composite has also been studied at 200 mA g^{-1} where after 50 charge-discharge cycles the charge capacity decreases from 323 to 70 mA h g^{-1} which is only 22% of its initial capacity (Figure S3B).

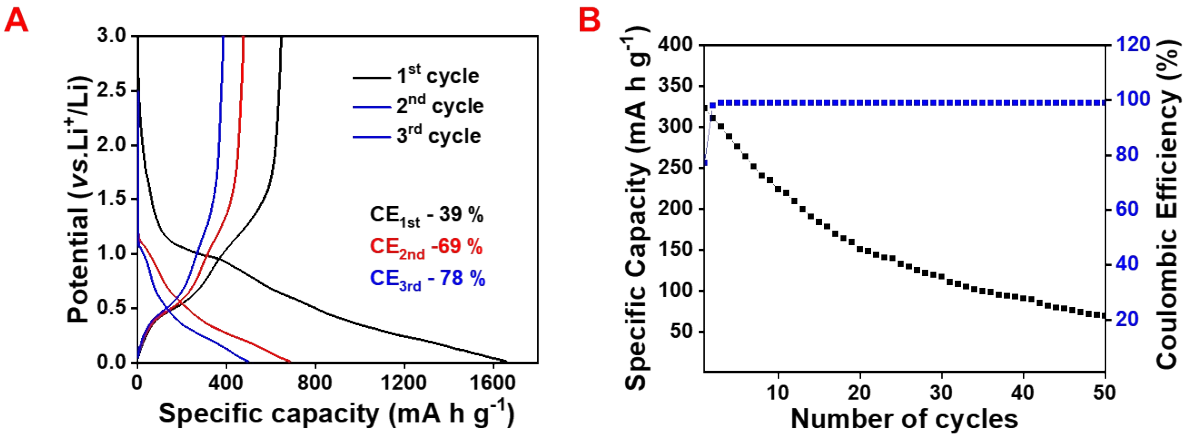

Fig. S3: (A) Charge-discharge profile and **(B)** cyclic stability of P-C/SnO_2 composite.

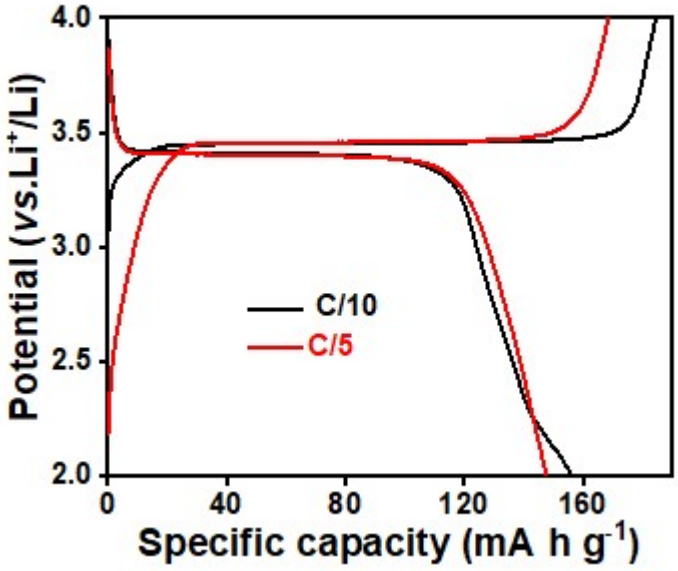

Fig. S4: Charge-discharge profile of C/LFP.

From the comparative EIS plot (Figure S5A) no significant change in R_S value is observed, but R_{CT} value is found to have increased significantly after the 100 charge-discharge cycles. R_{CT} value increases from 48 ohm to 447 ohm after 100 charge-discharge cycles complying with the low stability and rate of C/SnO_2 as NIB. The calculated diffusion co-efficient values of Na-ions for C/SnO_2 are relatively low which are 3.16×10^{-16} m^2 s^{-1} and 4.85×10^{-16} m^2 s^{-1} before and after the 100 charge-discharge cycles (Figure S5B and C).

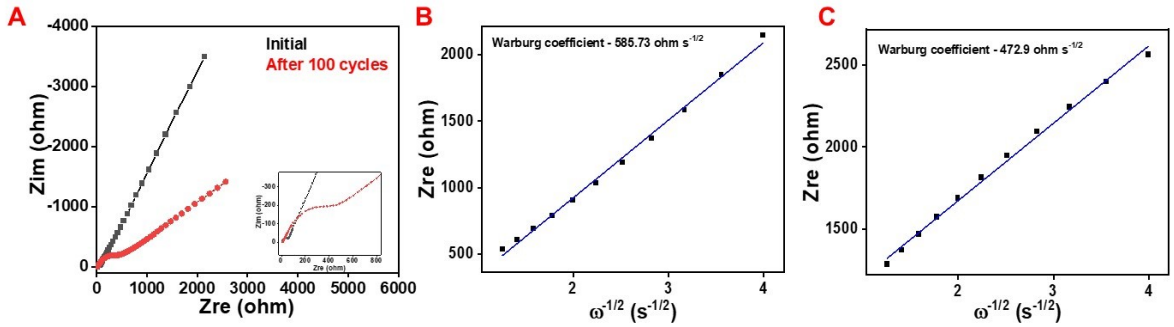

Fig. S5: Electrochemical performance of C/SnO_2 as Na-ion battery anode; **(A)** EIS curve before and after the 100 charge-discharge cycles, **(B & C)** real impedance (Z_{rel}) vs angular frequency (ω) plot before and after the 100 charge-discharge cycles, respectively.

Table 1: Comparative electrochemical performance of different reported carbon-SnO_2 composite as Li-ion battery anode with the as-prepared C/SnO_2 composite.

Composite	**Synthesis procedure**	**Specific capacity/mA hg^{-1} (current/ mA g^{-1})**	**ICE**	**Reference**
SnO_2/carbon	Wet-chemical followed by sacrificial template	697 (100)	49%	1
Core shell SnO_2/C	Hydrothermal	890 (100)	67%	2
Carbon/SnO_2	Calcination	837 (50)	53.4%	3
SnO_2/carbon nanofibre	Sol-gel	732 (100)	52.5%	4
Carbon coated SnO_2	Hydrothermal	948 (120)	71%	5
Carbon supported SnO_2	Electrodeposition	700 (100)	53%	6
C/SnO_2	Annealing	955 (200)	63%	7
C/SnO_2	Electrospinning followed by annealing	1124 (200)	72.9%	8
SnO_2/C nanospheres	Hydrothermal	1197 (100)	45%	9
N-doped carbon coated SnO_2	Hydrolysis	1082 (100)	75%	*10*
C@SnO_2@C	Hydrothermal	853 (200)	58%	*11*
C/SnO_2 nanowires	Wet chemical dispersion followed by annealing	868 (25) 608 (100)	52%	This work

Table S2: Calculated electrochemical impedance parameters of C/SnO_2 as LIB anode at different stages of the charge-discharge cycles.

	R_S (ohm)	**R_{CT} (ohm)**	**Warburg coefficient (ohm $s^{-1/2}$)**	**Diffusion constant (cm^2 s^{-1})**
Initial	2.9	62.1	89.2	1.36×10^{-14}
After 100 cycles	6.7	32.6	71.47	2.12×10^{-14}
After 500 cycles	7.4	48.3	27.13	1.47×10^{-13}

References:

1 W. Wang, P. Li, Y. Fu and X. Ma, *J. Power Sources*, 2013, **238**, 464–468.

2 J. Liu, W. Li and A. Manthiram, *Chem. Commun.*, 2010, **46**, 1437–1439.

3 Y. Li, Q. Meng, J. Ma, C. Zhu, J. Cui, Z. Chen, Z. Guo, T. Zhang, S. Zhu and D. Zhang, *ACS Appl. Mater. Interfaces*, 2015, **7**, 11146–11154.

4 M. Wang, S. Li, Y. Zhang and J. Huang, *Chem. Eur. J.*, 2015, **21**, 16195–16202.

5 X. W. Lou, J. S. Chen, P. Chen and L. A. Archer, *Chem. Mater.*, 2009, **21**, 2868–2874.

6 R. Hu, H. Zhang, J. Liu, D. Chen, L. Yang, M. Zhu and M. Liu, *J. Mater. Chem. A*, 2015, **3**, 15097–15107.

7 H. Wang, G. Jiang, X. Tan, J. Liao, X. Yang, R. Yuan and Y. Chai, *Inorg. Chem. Commun.*, 2018, **95**, 67–72.

8 Q. Wang, J. Xu, G. Shen, Y. Guo, X. Zhao, Y. Xia, H. Sun, P. Hou, W. Xie and X. Xu, *Electrochim. Acta*, 2019, **297**, 879–887.

9 X. Ao, J. Jiang, Y. Ruan, Z. Li, Y. Zhang, J. Sun and C. Wang, *J. Power Sources*, 2017, **359**, 340–348.

10 Y. Hong, W. Mao, Q. Hu, S. Chang, D. Li, J. Zhang, G. Liu and G. Ai, *J. Power Sources*, 2019, **428**, 44–52.

11 B. Cao, Z. Liu, C. Xu, J. Huang, H. Fang and Y. Chen, *J. Power Sources*, 2019, **414**, 233–241.